Surface Tensile Strength and Hertzian Fracture Resistance of Patterned Acid-Etched Glass

Datsiou, Kyriaki Corinna; Overend, Mauro

DOI
10.1061/JAEIED.AEENG-1464

Publication date
2023

Document Version
Final published version

Published in
Journal of Architectural Engineering

Surface Tensile Strength and Hertzian Fracture Resistance of Patterned Acid-Etched Glass

Kyriaki Corinna Datsiou[1] and Mauro Overend[2]

Abstract: Patterned acid-etched glasses are frequently used in horizontal glass surfaces that may be walked on, such as floors and staircase treads. These glasses provide useful antislip properties, but the foot traffic cause contact stresses and ageing mechanisms that are poorly understood and can affect the strength of the acid-etched glass. This study explores these strength-reducing effects by undertaking nondestructive and destructive evaluations of two acid-etched glasses with geometrically different surface patterns and comparing their mechanical performance to unetched float glass. In particular, residual surface stress, Hertzian fracture resistance, and fractographic characteristics are determined for each glass type. The surface tensile strength of the glasses is also evaluated by means of destructive flexural tests before and after artificial ageing. The flexural tests reveal that the ridge areas of the acid-etched surface patterns are more susceptible to the formation of digs and deeper surface flaws and are therefore weaker than both the valley areas of the acid-etched pattern and the surface of the unetched float glass. Correspondingly, the acid-etched glass with the highest proportion of ridges was more susceptible to ageing-induced flaws and had the lowest surface tensile strength. The contact (Hertzian) fracture resistance was also significantly affected by the presence of a surface pattern in the acid-etched glass; specifically, the lowest contact strengths were recorded for hard body contact on the ridges of the pattern. The fracture phenomena and new data presented in this paper provide useful insights on the long-term performance of etched patterned glass. The findings can provide the bases for real-world design decisions and for glass forensics. **DOI: 10.1061/JAEIED.AEENG-1464**.

Author keywords: Frosted glass; Acid-etched glass; Patterned glass; Strength; Ageing; Hertzian fracture; Foot traffic; Hard-body contact strength; Glass fracture interpretation.

Introduction

Patterned glass is commonly used in architectural applications to meet aesthetic requirements or to provide privacy (e.g., partition walls, doors) without significantly compromising light transmission. The pattern on glass can be created by: (1) rolling the molten glass between two rollers to impress a design onto the glass surface, known as rolled patterned glass; (2) selective removal of parts of the glass surface by mechanical abrasion at ambient temperature, referred to as sandblasted glass; and (3) selective removal of parts of the glass surface by chemical treatment at ambient temperature, commonly known as acid etching. The latter involves hydrofluoric (HF) acid solutions to superficially erode the surface of the glass and typically provides a smoother finish compared with sandblasted glass and is also less prone to fingerprint accumulation. The dissolution of the glass surface occurs as the HF acid reacts with the silica at surface of the glass leading to the formation of hexafluorosilicic acid or silicon tetrafluoride depending on the process temperature, which can be shown as (Kolli et al. 2009; Spierings 1993)

$$SiO_2 + 6HF \rightarrow H_2SiF_6 + 2H_2O \text{ for } T < 60^\circ C \quad (1)$$

$$SiO_2 + 4HF \rightarrow SiF_4 + 2H_2O \text{ for } T \geq 60^\circ C \quad (2)$$

The dissolution of the glass is only terminated when the solution is removed or when the HF reactant is fully converted to the reaction products. Alternatively, when salts (e.g., NH_4HF_2) are present in the acidic solution, the silicon that diffuses from the glass reacts with the salt forming a protective/passivating layer that prevents further glass dissolution (Barboux et al. 2004; Piret et al. 2018), which can be presented as

$$SiF_4 + 2HF + 2NH_4 \rightarrow (NH_4)_2SiF_6 + 2H^+ \quad (3)$$

This layer grows and gradually extends across the surface of the glass, as it is continuously fed by the silicone diffusing from the glass and the NH_4^+ cations in the solution.

The etching process leads to the formation of a network of elevations on the glass surface that resembles a crystal-like arrangement (Barboux et al. 2004). This is the result of the dual mechanism of the dissolution of the glass and the 2D growth of the passivating layer that prevents further dissolution. The surface roughness, dissolution depth, light transmission, and surface morphology of the glass are influenced by a combination of parameters: (1) etchant composition (concentration of HF, the addition of other strong acids such as HCl, HNO_3, or H_2SO_4 or salts in the mixture); (2) chemical composition of the glass; and (3) duration of the acid treatment (Frayret et al. 2008; Jang et al. 2000; Kolli et al. 2009; Maeng et al. 2014; Spierings 1993).

Surface patterns can be introduced by strategically masking areas of the glass surface thereby protecting these areas from etching while depths of material are removed (etched) from the unprotected areas. The resulting protrusions increase surface friction,

[1]Senior Lecturer, Centre for Engineering Research, School of Physics, Engineering and Computer Science, Univ. of Hertfordshire, Hatfield AL10 9AB, UK (corresponding author). ORCID: https://orcid.org/0000-0002-6672-535X. Email: k.c.datsiou@herts.ac.uk

[2]Professor, Dept. of Architectural Engineering & Technology, TU Delft, Delft 2628 BL, Netherlands. ORCID: https://orcid.org/0000-0001-5929-497X. Email: m.overend@tudelft.nl

Note. This manuscript was submitted on March 7, 2022; approved on March 10, 2023; published online on May 5, 2023. Discussion period open until October 5, 2023; separate discussions must be submitted for individual papers. This paper is part of the ***Journal of Architectural Engineering***, © ASCE, ISSN 1076-0431.

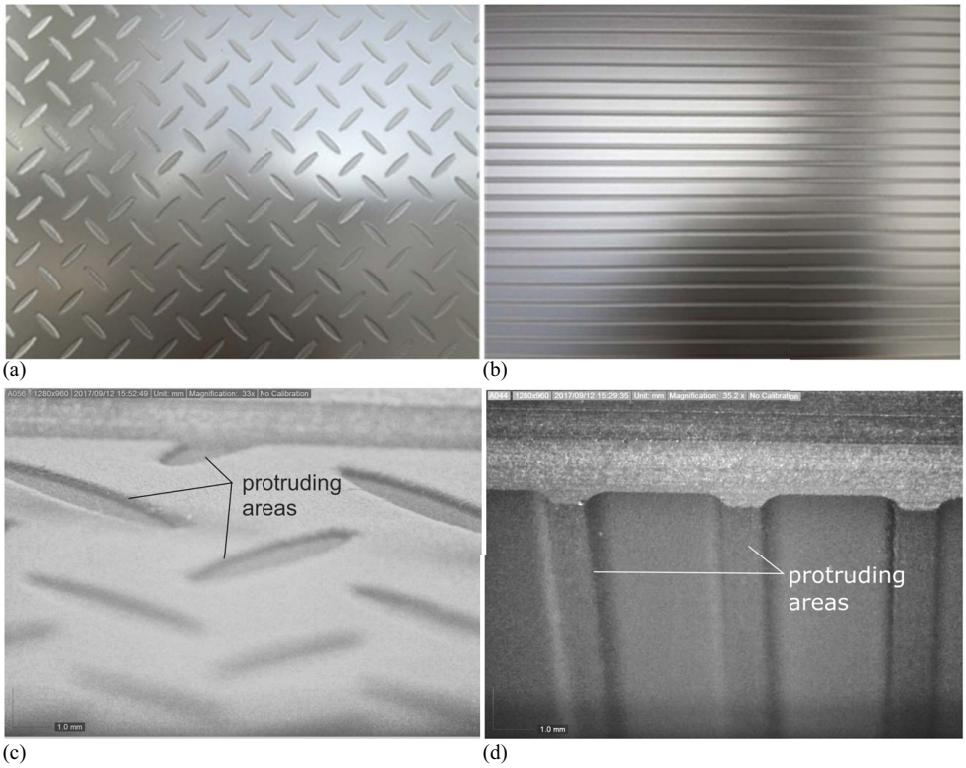

Fig. 1. Top and side views of acid-etched glass for (a and c) diamond (ED) pattern; and (b and d) linear (EL) pattern.

providing antislip properties to the glass. Patterned acid-etched glass is therefore commonly used for walking surfaces accessible to the public, such as glass staircases or walkways. The glass units used in such applications are frequently multilayered laminated glass, therefore catastrophic failure is uncommon, but chips, local cracks, and large fractures frequently occur in the top (acid-etched) layer of glass; the replacement of which typically incurs significant disruption and costs.

Previous research has shown that it is possible to increase glass strength with acid treatment, despite the associated reduction in the thickness of the glass. The acid treatment removes the surface layer of the glass and blunts the pre-existing flaw tips, thereby reducing the stress-raising effects of the flaws (Dabbs and Lawn 1982; Kolli et al. 2009; Maeng et al. 2014; Wang et al. 2020). The extent of this improvement depends on the depth of the dissolved glass layer and the morphology of pre-existing flaws. In addition, even when all pre-existing surface flaws are removed, the strength of the glass in turn depends on the presence of flaws located within the bulk of the glass that may become exposed after etching. Most literature to date focuses on the effect of acid etching on the strength recovery of glass containing surface flaws (Dabbs and Lawn 1982; Kolli et al. 2009; Maeng et al. 2014; Wang et al. 2020). However, there is a lack of information on the strength or fracture resistance of patterned acid-etched glass, including the long-term performance after exposure to ageing mechanisms. Standardized wear resistance tests for other materials exist; for example, the Taber abrasion test on ceramics in ASTM C501 (ASTM C501-21, ASTM 2021a). However, the standardized tests rank materials in terms of their relative wear resistance by measuring the mass loss after abrasion, but they fail to provide any information on the long-term strength of the abraded material and the abrasion process used in these standardized tests is not representative of foot traffic on glass surfaces.

The present study addresses this directly by investigating the mechanical performance of two types of acid-etched glass with geometrically different surface patterns (linear and diamond) and comparing this to unetched glass. In particular, tests are performed to determine their strength characteristics in their as-received (AR) and artificially aged (AA) state as well as their resistance to Hertzian fracture. A controlled and repeatable artificial ageing process, using mechanical abrasion, is selected and used in this study. In addition, Hertzian fracture tests are undertaken to simulate and investigate the effects of flaws induced by grit/gravel that could be pressed by pedestrians' footwear thereby inducing Hertzian stresses on the glass surface, that is, localized stresses that develop as the gravel comes into contact with the glass under the imposed loads. The glass types selected for this study and the experiments used to characterize the glass are described in the sections "Materials" and "Methods," respectively. The results and salient observations from the experimental testing on acid-etched glass are presented in the section "Results and Discussion" while the section "Conclusions" summarizes important conclusions.

Materials

Three types of annealed, soda lime silica glass were investigated: (a) unetched soda lime silica, float glass (U series); (b) acid-etched glass with a diamond surface pattern [ED series, Figs. 1(a and c)]—this pattern is commonly used in the building industry due to its antislip properties and; (c) acid-etched glass with a linear surface pattern [EL series, Figs. 1(b and d)] that can be used as an alternative to ED glass. The tin and air side of the specimens were identified using an ultraviolet light tin-side detector. It was found that the etching (in series ED and EL) was always performed on the air side and, therefore, the air side of the unetched float (U) series was also used in subsequent tests for consistency.

Table 1. Series of specimens for flexural strength tests

Glass type	Dimensions (mm)	No. of specimens	Ageing	Series
Unetched	150 × 150 × 8	15	As-received	U-AR
		15	Artificially aged	U-AA
Acid-etched – diamond pattern	150 × 150 × 8	15	As-received	ED-AR
		15	Artificially aged	ED-AA
Acid-etched – linear pattern	150 × 150 × 8	15	As-received	EL-AR
		15	Artificially aged	EL-AA

Table 2. Series of specimens for Hertzian fracture resistance tests

Glass type	Dimensions (mm)	No. of specimens	Processing	Contact location	Series
Unetched	150 × 150 × 8	6	As-received	NA	U-AR
Acid-etched – diamond pattern	150 × 150 × 8	6	As-received	Valley	ED-AR-V
			As-received	Ridge	ED-AR-R
Acid-etched – linear pattern	150 × 150 × 8	6	As-received	Valley	EL-AR-V
			As-received	Ridge	EL-AR-R

Each type of glass was investigated in its AR and AA state in terms of flexural strength while AR specimens were used to identify the resistance to Hertzian fracture.

A total of 90 specimens were tested to investigate flexural strength (Table 1); 15 nominally identical specimens per glass type (U; ED; EL), per ageing condition (AR; AA). The series size of 15 was selected to reduce uncertainty in strength estimates during the statistical analysis of strength data following the recommendations in Datsiou (2017).

A total of 18 specimens were used to investigate the resistance of glass to Hertzian fracture in the AR state (Table 2); six specimens were used per glass type (U-AR, ED-AR, EL-AR). Both valley and ridge contact locations were investigated for the two types of acid-etched glass (R; V, for contact at the ridge and valley locations, respectively). Specimens used for ridge contact tests were reused for valley tests (refer to the section "Hertzian Fracture" for more details).

Methods

The nondestructive and destructive tests performed in this study are described in the following subsections.

Residual Stress Measurements

All specimens were examined with a scattered light polariscope SCALP-05 (GlasStress Ltd.) to determine the residual surface stress through the thickness of the glass. Three surface readings were taken at the center of each specimen in two orthogonal directions. The original intention was to take a reading on the etched surface but this was not possible with the current equipment, so a reading on the other surface (tin side) was taken. This provided a measure of residual stresses in the entire glass specimen, but it was not a good indicator of the residual stresses on the acid-etched surface.

Artificial Ageing

The wear resistance of ceramics is typically evaluated using Taber abrasion tests based on ASTM C501 (ASTM C501-21, ASTM 2021a). However, this approach was not deemed appropriate for this study as: (1) there is no published research on the correlation between the damage induced with the Taber abrasion test and the damage induced by foot traffic in real-world applications; and (2) the evaluation is based on mass loss rather than strength reduction.

A falling abrasive method, similar to the approach described in DIN 52348 (DIN 52348, DIN 1985) and ASTM D968-05 (ASTM D968-05, ASTM 1991) was used instead. One series (15 specimens) from each type of glass was artificially aged. The artificial ageing parameters (Table 3) were adjusted to produce a relatively small scatter in strength data with the introduction of a small percentage of gravel in the abrasive medium according to recommendations in Datsiou and Overend (2017). Their artificial ageing method produced good correlation to the level of damage found in naturally aged, annealed glass exposed to 20 years of weathering in a facade in Norfolk, UK. It should be noted that this ageing process is calibrated for vertical facades, but in the absence of data on ageing characteristics of glass floors, this method was selected in this study. While it is uncertain whether this is representative of ageing of floors, it provides a controlled and repeatable means of artificial ageing that is essential for this study.

In summary, the method involves dropping an abrasive medium (mix of rounded silica sand and riverside gravel, grain size distribution shown in Fig. 2) from a specified height on the surface of the specimen (Table 3), which is clamped to a rotating base at an angle of 45° to the floor. The air surface in the unetched glass and the corresponding patterned surface in the acid-etched glass were exposed to ageing.

Visual Inspection and Optical Microscopy

Qualitative micrographs of the edge and the surface of AR and AA glass were obtained with a digital Dino-Lite digital microscope and a Leica DM ML optical microscope, for low magnification and high magnification micrographs, respectively.

Table 3. Artificial ageing parameters

Artificial ageing parameter	Value
Drop height	3 m
Abrasive medium	Riverside gravel and silica sand
Total mass of abrasive medium	3,000 g
Percentage of gravel	0.1%
Grain size range of sand	0.5–0.7 mm
Grain size range of gravel	8.0–9.5 mm
Rotation rate	250 rpm
Elapsed time to destructive test	1 day

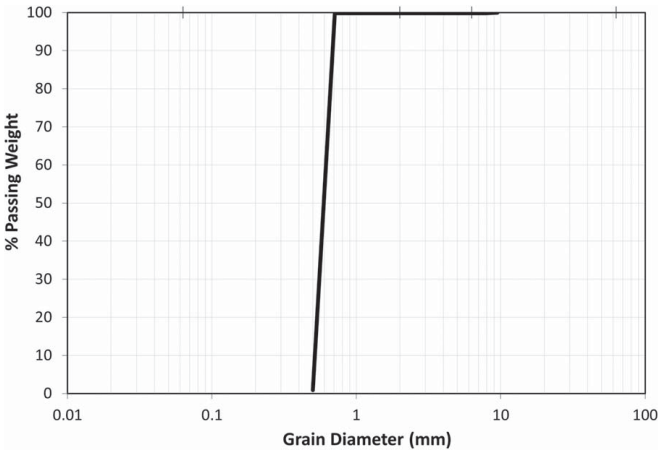

Fig. 2. Grain size distribution of abrasive medium.

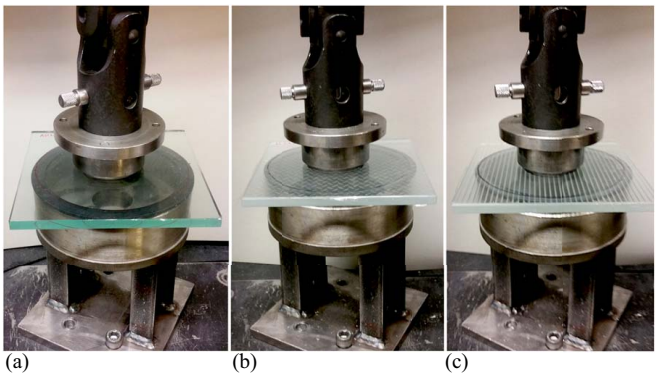

Fig. 3. Destructive CDR test for (a) U; (b) ED; and (c) EL glass series.

Destructive Tests and Statistical Analysis of Strength Data

Prior to the destructive testing, a self-adhesive film was applied on the compression surface of the glass to retain the glass fragments after failure thereby permitting fractographic analysis (section "Fractography"). The strength of the glass specimens was assessed using a coaxial double ring setup (CDR, Fig. 3) using the loading and the reaction ring of $D_L = 51$ mm and $D_R = 127$ mm in compliance with ASTM C1499-03 (ASTM C1499-03, ASTM 2009). The loading ring was connected to a 30 kN electromechanical universal testing machine by means of an articulated joint to ensure an even contact between the loading ring and the specimen's surface. A 2 mm-thick rubber ring was introduced on the reaction ring to ensure uniform contact between the reaction ring and the pattern glass surface. The specimens were oriented so that the air side of the glass (i.e., the patterned surface of the acid-etched specimens) was in tension during the destructive testing. A stress rate of 20 MPa/s, corresponding to a displacement rate of 13.6 mm/min, was selected to induce fast fracture, thereby minimizing the influence of subcritical crack growth in the glass and achieving quasi-inert conditions (Overend and Zammit 2012).

To assist the experimental testing, a finite-element analysis (FEA) model of the CDR testing of glass (Poisson's ratio $\nu = 0.23$ and Young's modulus $E = 70$ GPa) was created in Abaqus-Dassault Systèmes v.6.12 to determine the failure stress corresponding to the recorded failure load. The model was in line with the one described in Datsiou and Overend (2017), consisting of 6,774 quadratic quadrilateral shell elements (S8R) and considered friction between the loading/reaction ring and the glass specimen. The FEA model revealed that the tension surface circumscribed by the loading ring was subjected to an equibiaxial state of stress, with no significant stress concentrations below the loading ring. The model of a 150×150 mm glass specimen with a thickness of 7.95 mm (matching the mean thickness of the unetched and etched glasses) showed a linear relationship between the failure load and failure stress, which is described by

$$\sigma_1 = 0.010 \cdot P + 0.164 \tag{4}$$

where σ_1 (MPa) = principal stress; and P (N) = failure load.

The intercept in Eq. (4) corresponds to the self-weight of the glass and the 15 N preload used to align the loading ring on the surface of the glass specimen.

The ramp stress history exerted during the destructive tests was subsequently converted to a uniform equivalent stress history ($\sigma_{f,60}$, for a reference time period, t_{ref}, of 60 s) that causes the same level of crack growth, using

$$\int_0^{t_f} \left(\frac{\sigma_f \cdot t}{t_f}\right)^n dt = \int_0^{t_{\text{ref}}} \sigma_{f,60}^n dt \Rightarrow \sigma_{f,60} = \sigma_f \cdot \left[\frac{t_f}{t_{\text{ref}} \cdot (n+1)}\right]^{1/n} \tag{5}$$

where σ_f = failure stress; and n = exponential crack velocity parameter also known as static fatigue constant [$n = 16$ for normal environmental conditions (Haldimann et al. 2008)]. This approach normalizes the effects of any remaining subcritical crack growth for specimens failing at different times.

The resulting equivalent strength data were then statistically analyzed and a two parameter Weibull distribution [Eq. (3)] was fitted to determine salient strengths, which can be represented as

$$P_f(\sigma_{f,60}) = 1 - \exp\left[-\left(\frac{\sigma_{f,60}}{\theta}\right)^{\beta}\right] \tag{6}$$

where P_f = probability of failure; β = shape factor; and θ = scale factor of the Weibull distribution.

A weighted least-squares regression method using Hazen's probability estimator and Faucher and Tyson's weight function was used in this study to compute the Weibull characteristics following the approach described in detail in Datsiou and Overend (2017, 2018). The Anderson Darling method, p_{AD}, with a 5% confidence level was used to determine the goodness of fit. With a known cumulative distribution function (CDF), salient strength values can then be obtained, such as for engineering design purposes [$P_f = 0.008$ according to ASTM E1300-16 (ASTM E1300-16, ASTM 2016)] and mean probabilities of failure ($P_f = 0.50$).

Fractography

Fractured surfaces were analyzed with a Leica DM ML optical microscope, after destructive testing to determine the origin of failure and the critical flaw. Wallner lines pointed toward the direction of the critical flaw; the mirror, mist, and hackle revealed its precise location (Quinn 2007).

Hertzian Fracture

Patterned acid-etched glass has useful antislip properties and is commonly used in floors and other walking surfaces. During its service-life, it is likely that grit/gravel on the glass or trapped in pedestrians' footwear, is pressed onto the surface of the glass, potentially causing (Hertzian) fracture of the glass. To investigate this effect, Hertzian fracture investigations are undertaken for all three glasses considered in this study. All tests were performed on AR (unaged) glass.

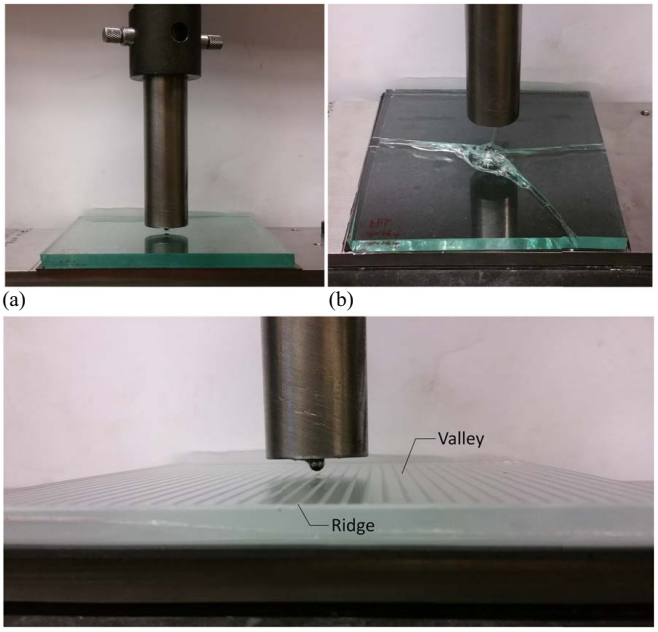

Fig. 4. Hertzian fracture: (a) setup; (b) indicative fracture in unetched float glass; and (c) close-up of ball bearing on EL glass.

The Hertzian fracture was induced by pressing a spherical ball bearing on the surface of the glass [Figs. 4(a and c)] to induce a localized stress field and a subsequent subsurface conical crack [Fig. 4(b)]. The unloaded (bottom) surface of the glass was supported continuously by a thick steel plate placed on a stiff lower baseplate of a 30 kN electromechanical test machine; an intermediate 2 mm-thick rubber sheet was placed between the specimen and the steel plate to ensure even support of the glass plate. The ball bearing was made of hardened carbon steel, had a diameter of 5 mm, and was fitted to a cylindrical steel strut that was in turn attached to the crosshead of the 30 kN test machine. An initial preload of 15–18 N was applied on the glass at a speed of 4 mm/min in order to achieve contact between the specimen and the indenter. The test subsequently proceeded at a displacement rate of 8 mm/min until fracture.

The indentation was applied to the air surface of the unetched and the patterned surface of the acid-etched glass. Prior to the test, the ball bearing was aligned with: (1) the center of the specimen for the unetched float glass; (2) the "ridge" closest to the center of the specimen for the ED and the EL glasses. After the first Hertzian fracture was induced on the ED and the EL glass, the ball bearing was repositioned over a "valley" at a distance of at least 20 mm away from the first fracture and the test was repeated to determine the valley Hertzian fracture resistance.

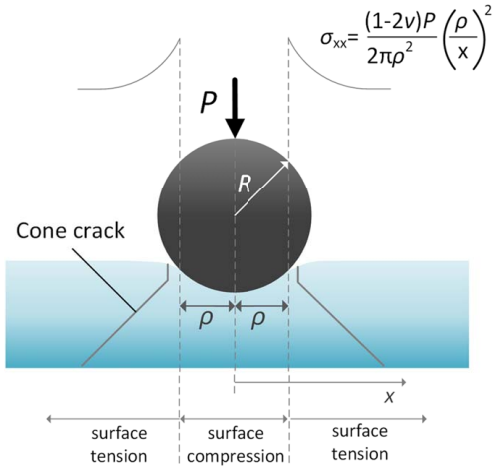

Fig. 5. Hertzian cone fracture and principal tensile stress profile.

During the test, the load P (N) was distributed over a circular (on plan), contact region between the ball bearing and the glass (Fig. 5). The radius of which is known as the contact radius, ρ (mm), and is given by (Fischer-Cripps 1997; Wilshaw 1971)

$$\rho = \left(\frac{4}{3}\cdot\frac{k\cdot P\cdot R}{E}\right)^{1/3} \tag{7}$$

where $R = 2.5$ mm = radius of the ball bearing; $E = 70$ GPa = Young's modulus of the glass; and k = factor composed of the elastic constants of the hardened carbon steel indenter and the glass, which can be represented as

$$k = \frac{9}{16}\left((1-\nu^2)+(1-\nu_{\text{ball}}^2)\frac{E}{E_{\text{ball}}}\right) \tag{8}$$

where the Poisson's ratio of the glass is $v = 0.23$; the Poisson's ratio for the ball bearing is $v_{\text{ball}} = 0.28$; and the Young's modulus of the ball bearing is $E_{\text{ball}} = 200$ GPa.

The maximum tensile surface stress occurs at $x = \pm\rho$ (Fig. 5), that is, at the contact circle boundary and is given by (Fischer-Cripps 1997; Wilshaw 1971)

$$\sigma_{\max} = \frac{1-2v}{2}\cdot\frac{P}{\pi\cdot\rho^2} \tag{9}$$

The major principal stresses, σ_{xx}, are oriented radially and decrease with distance from the contact circle boundary. In this study, the stresses resulting from Eq. (9) were converted to an equivalent fracture stress for a reference time of 60 s as described in section "Destructive Tests and Statistical Analysis of Strength Data."

Table 4. Residual surface stress results

Glass type	Orthogonal direction	Mean surface stress σ_{RES} (MPa)	Standard deviation	Variance	Max surface stress (MPa)	Min surface stress (MPa)	Coefficient of variance	Mean total surface stress (MPa)
Unetched glass U series	x	−4.49	0.55	0.31	−3.49	−5.81	0.12	−4.42
	y	−4.35	0.55	0.30	−3.28	−5.48	0.13	
Acid-etched diamond	x	−3.73	1.04	1.08	−1.61	−6.19	0.28	−3.74
ED series	y	−3.75	0.79	0.63	−2.02	−5.46	0.21	
Acid-etched linear EL	x	−4.06	0.86	0.73	−2.72	−6.04	0.21	−4.03
series x	y	−4.00	0.91	0.82	−2.16	−5.46	0.23	

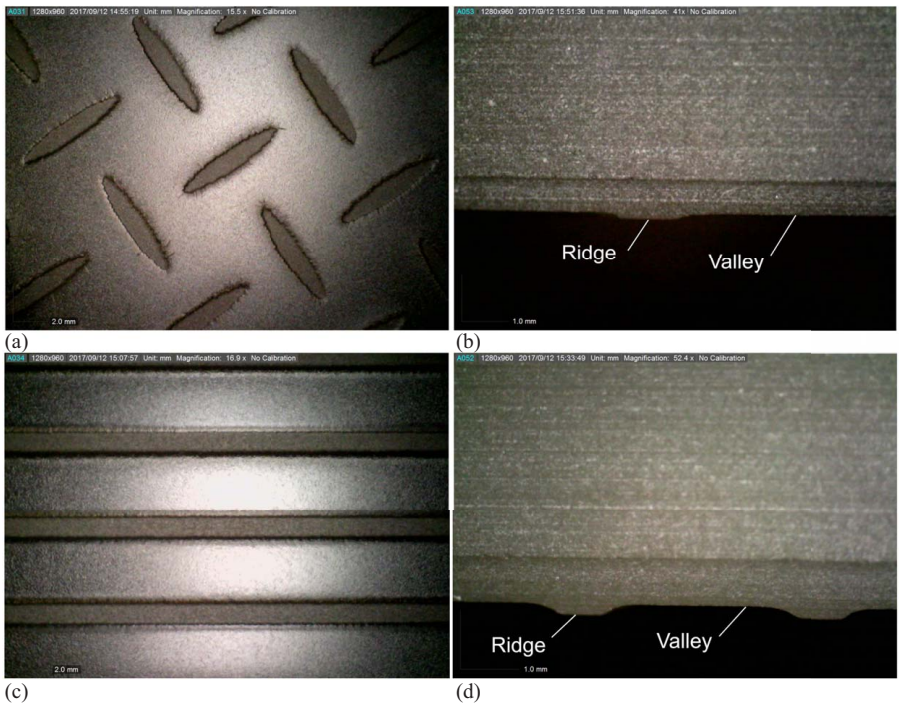

Fig. 6. Surface and edge pattern of (a and b) ED; and (c and d) EL glass.

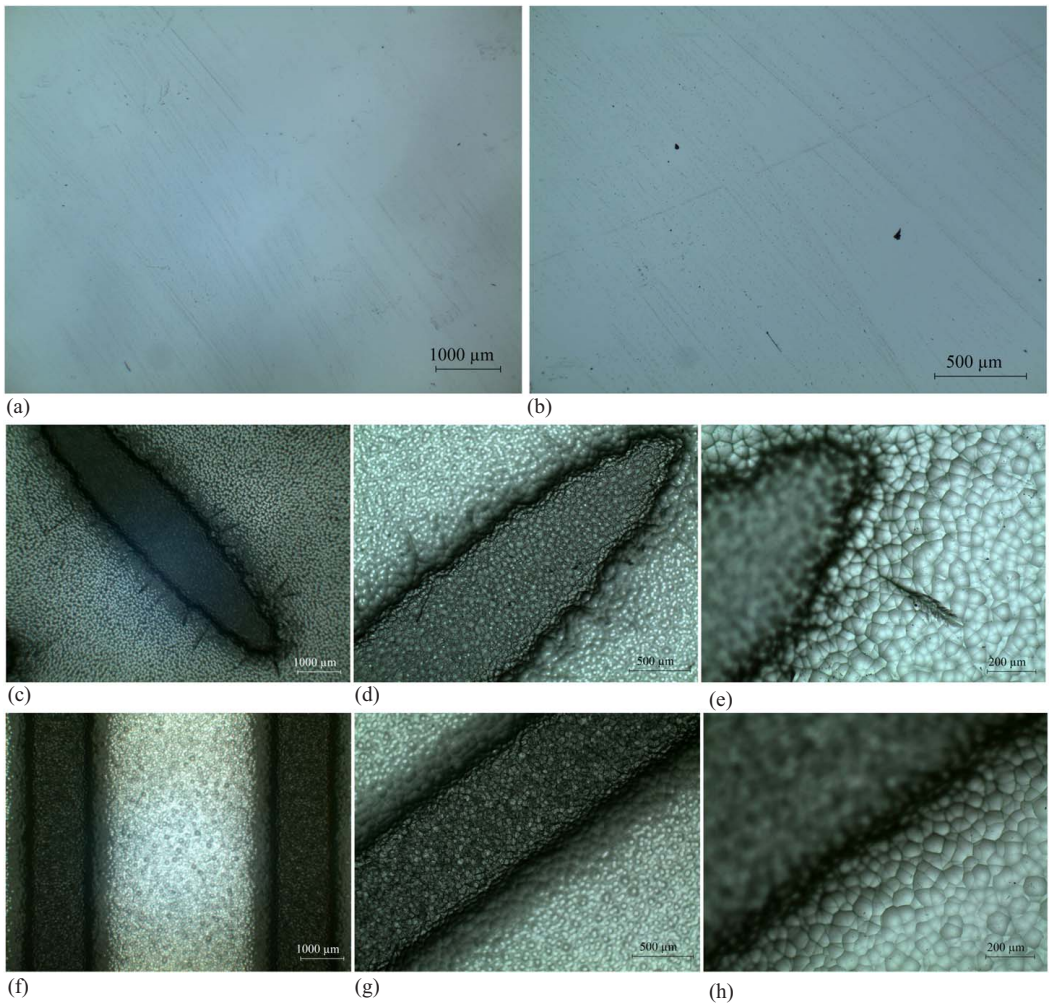

Fig. 7. Micrographs of AR: (a and b) U glass; (c–e) ED glass; and (f–h) EL glass at different levels of magnification.

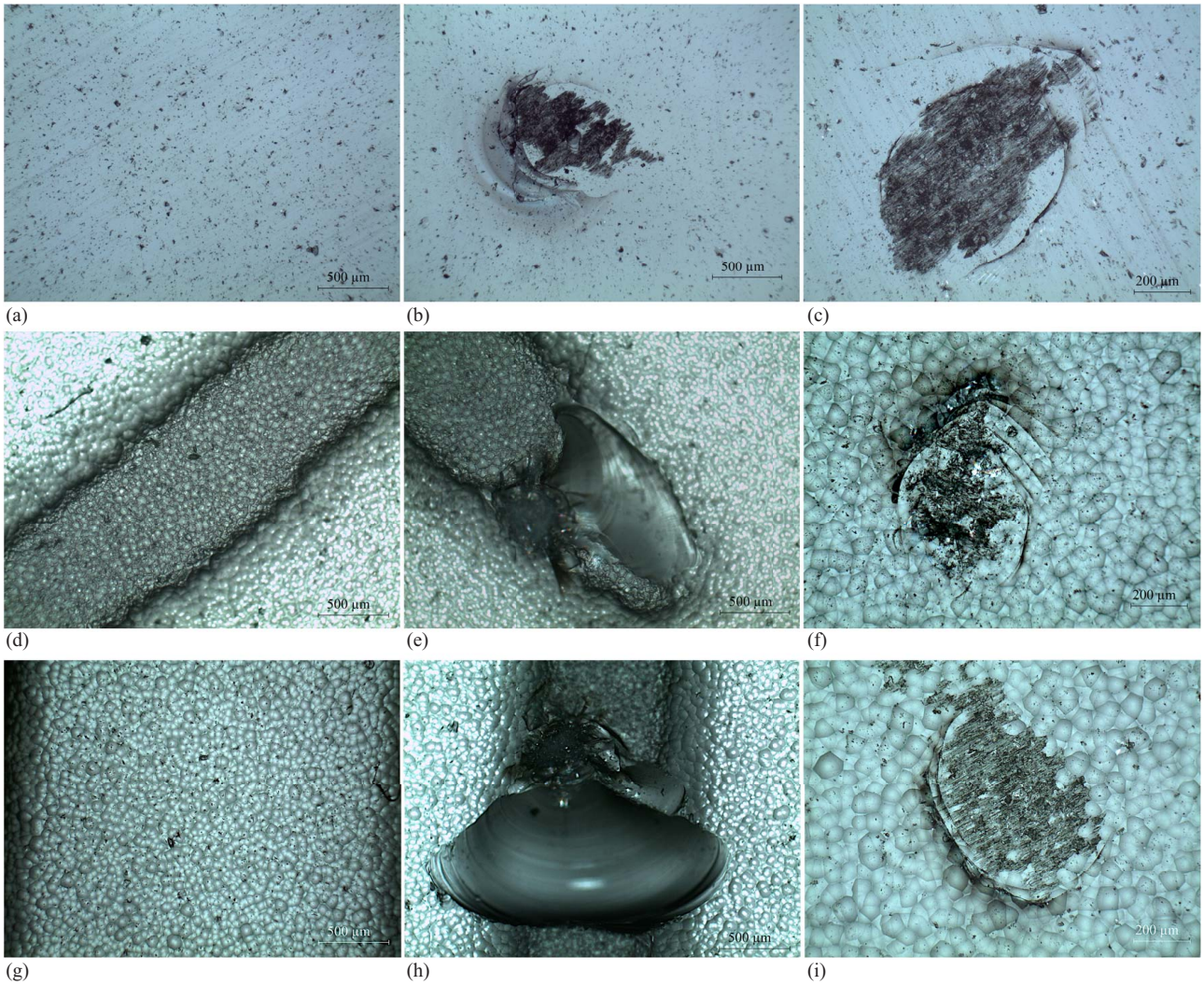

Fig. 8. Micrographs of abraded: (a–c) F glass; (d–f) ED glass; and (g–i) EL glass.

Results and Discussion

Residual Stress Measurements

A summary of the residual surface stress results obtained for each type of glass is presented in Table 4. This shows mean values in two orthogonal directions, extreme values, standard deviation, and variance and coefficient of variance for each type of glass.

The results do not reveal any abnormal stresses on the untreated surfaces of the glass types investigated in this study. All specimens had a small level of residual surface compression (σ_{RES}), which is within the expected compressive range for commercial annealed glass [$0 \geq \sigma_{RES} \geq -11$ MPa (Haldimann et al. 2008)]. In addition, there are no significant differences between the stresses in the two orthogonal directions.

The mean surface stress reported in Table 4 corresponds to the untreated surface of the acid-etched glass. From these, it is not possible to infer the residual stress state of the acid-etched surface and in particular whether residual surface tension is present within a shallow depth of the acid-etched surface.

Visual Inspection and Microscopy

The treated surface of the ED series consists of a regular pattern of raised elliptical "diamonds" or "bars" on the air side [Fig. 6(a)] and a featureless flat tin side, in a similar manner to steel chequer plates. The treated surface of the EL series consists of a regular pattern of linear raised stripes on the air side [Fig. 6(c)] and a featureless flat tin side. The ratio of the ridge surface area over the total surface area is 15% and 38% approximately for the ED and the EL series, respectively. The ridges are relatively smooth with filleted corners and at this scale [magnification of ×41 for Fig. 6(b) and ×52 for Fig. 6(d)] there is no evidence of any sharp edges or re-entrant corners that could act as stress-concentration features.

Representative optical micrographs of the surface of all glass types in their AR and AA state are shown in and Figs. 7 and 8, respectively.

AR Glass

Minor scratch patterns and few pits are apparent on the surface of AR unetched float glass. The ED and EL micrographs reveal a dense network of semi/partly spherical surface features that are attributed to the acid treatment [Figs. 7(c–h)]. These features are responsible for diffusing incident light leading to the frosted appearance of the glass. Multiple feather-shaped flaws originate from the diamond pattern at the ridge–valley interfaces for the ED glass [Figs. 7(c and e)]. However, such flaws are not apparent in the EL glass [Figs. 7(f and h)], suggesting a higher glass quality. The underlying reasons for such flaws are not clear but could be related to one or a combination of the following: impurities in the

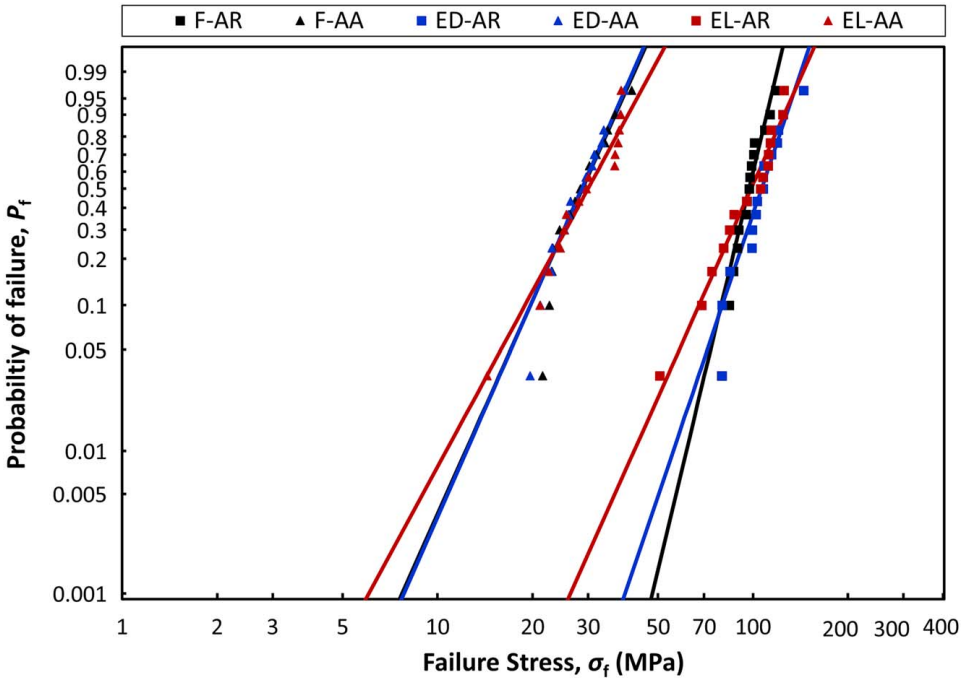

Fig. 9. CDFs for AR and AA series for all types of glass.

glass acting as nucleation points, handling of the glass, or etching process characteristics.

AA Glass

The surface defects known as pits or digs resulting from the sand impacts are of similar size in all types of glass [Figs. 8(a, d, and g)]. Gravel impacts at valley locations for acid-etched glass, create radial/median cracks and are of similar size in all types of glass [Figs. 8(c, f, and i)]. Surface chipping also known as chips and digs in ASTM C1036 (ASTM C1036-21, ASTM 2021b) was noticed where gravel impacts had occurred on ridges for both etched glasses [Figs. 8(e and h)].

Destructive Tests and Strength Data

The CDFs of the failure stress data are shown in Fig. 9. The corresponding Weibull parameters and the failure stress at salient probabilities of failure are summarized in Table 5.

AR Glass

The etched diamond pattern glass (ED-AR) and the etched linear pattern glass (EL-AR) were found to be 10% and 33% weaker than the unetched float glass (U-AR), respectively, at low probabilities of failure ($P_f = 0.008$). The strength reduction of ED-AR glass is within BS EN16612:2019 (BS EN 16612, BSI 2019) recommendations to use a surface profile reduction factor of $k_{sp} = 0.75$ on the design bending strength of annealed pattern glass, implying a 25% strength reduction. The design strength of the EL-AR glass in this study is below this threshold.

Conversely, at mean probabilities of failure, the strength of the acid-etched series exceeded that of unetched float glass with the highest values reported for the ED-AR series. ED-AR in particular, had a mean strength that was 10% higher and 8% higher than the U-AR and EL-R series, respectively.

The Weibull shape factor (β) that represents the gradient of the CDF is an inverse indicator of the scatter in strength data. Higher values of β were reported for U-AR glass, followed by the ED-AR glass and subsequently by the EL-AR glass, indicating that the EL-AR strength data has a larger scatter compared to the other two types of glass.

The etched linear pattern glass (EL-AR) had a higher data scatter and lower strength compared with the etched diamond pattern glass (ED-AR). This could be potentially attributed to the higher ratio of ridge area-to-total surface area (38% versus 15%), an indication that ridges in patterned glass might be weaker and more prone to damage accumulation due to their exposed nature.

AA Glass

The CDFs for the ED-AA and U-AA glass were nearly identical (Fig. 9). The etched linear pattern glass (EL-AA) was 15% lower than the other two glasses (U-AA and ED-AA) at low probabilities of failure ($P_f = 0.008$). However, the percentage reduction in

Table 5. Statistical analysis surface tensile strength results

Series	Design strength ($P_f = 8‰$) $\sigma_{0.008}$ (MPa)	Mean strength ($P_f = 50\%$) $\sigma_{0.50}$ (MPa)	Max strength max σ (MPa)	Min strength min σ (MPa)	Shape factor β	Scale factor θ
U-AR	59.99	97.05	117.88	79.44	9.27	100.96
U-AA	11.74	28.77	41.29	21.51	4.97	30.97
ED-AR	53.96	106.34	144.63	79.75	6.57	112.44
ED-AA	11.82	28.59	39.15	19.64	5.05	30.75
EL-AR	40.14	98.52	125.18	50.59	4.96	106.07
EL-AA	10.08	29.98	38.23	14.33	4.09	32.79

Table 6. Fractography results

Glass	Specimen	Flaw morphology	Radial/median crack	Flaw depth α (μm)	Flaw location
Unetched	U-AR2	Semielliptical	No	31	n/a
	U-AR8	Semielliptical	No	45	n/a
	U-AA9	Semielliptical	No	478	n/a
	U-AA11	Irregular	Yes	1,001	n/a
	U-AA12	Semielliptical	Yes	437	n/a
	U-AA15	Trapezoidal	No	322	n/a
Acid-etched diamond	ED-AR1	Semielliptical	No	50	Ridge
	ED-AA4	Semielliptical chip	No	383	Ridge
	ED-AA10	Semielliptical	No	209	Valley
	ED-AA12	Half penny	No	917	Ridge–valley interface
	ED-AA13	Trapezoidal	Yes	480	Valley
	ED-AA15	Trapezoidal	No	551	Ridge–valley interface
Acid-etched linear	EL-AR1	Half penny	No	62	Ridge
	EL-AR11	Half penny	No	23	Valley
	EL-AR12	Semielliptical	No	20	Ridge
	EL-AA3	Half penny	Yes	72	Valley
	EL-AA7	Semielliptical	Yes	380	Valley
	EL-AA9	Irregular	Yes	732	Valley
	EL-AA10	Irregular	Yes	3,810	Ridge–valley interface
	EL-AA11	Semielliptical	No	585	Valley
	EL-AA12	Semielliptical chip	No	207	Ridge
	EL-AA14	Trapezoidal	Yes	595	Ridge
	EL-AA15	Semielliptical	No	39	Valley

strength from AR to AA was similar for all types of glass at low probabilities of failure ($P_f = 0.008$), namely 80% for the unetched float glass, 78% for the ED glass and 75% for the EL glass. Similar to AR glass, the shape factor for the EL-AA glass was smaller than that of the other two types, indicating a larger scatter in glass strength data for this type of glass.

Fractography

Fractography was only possible for a small number of AR specimens because the high loads required to induce fracture in AR glass resulted in high-density fragmentation and associated high-energy release that tore the self-adhesive film intended to hold the fragments together, thereby making it difficult to recover the fragments containing the fracture origin. The fractography results are summarized in Table 6. Figs. 10 and 11 show typical examples of critical flaws found in AR and AA glass for each type of glass.

AR Glass

The results showed that the critical flaws were either half-penny [i.e., semicircular (Lawn 1993)] or semielliptical in shape. The following depths were measured for each type of glass (mean values are used where more than one specimens were available): $\alpha =$ 38 μm for unetched float (U-AR), $\alpha = 50$ μm for the etched diamond pattern glass (ED-AR), and $\alpha = 35$ μm for the etched linear pattern (EL-AR) glass. Large discrepancies in critical flaw sizes are observed for the EL series. This supports the scatter in the strength data for the EL series reported in the section "Destructive Tests and Statistical Analysis of Strength Data."

AA Glass

The shape of the critical flaws in this case varies (semielliptical, half-penny, or irregular) as it depends on the impact angle of the gravel during contact with the glass. The mean depth was $\alpha = 560$ μm for the unetched float glass (U-AA), $\alpha = 508$ μm for the etched diamond pattern glass (ED-AA), and $\alpha = 803$ μm for the etched linear pattern glass (EL-AA) glass.

The critical flaws located on ridges or at the interface between ridge and valley of the acid-etched glass for both ED-AA and EL-AA glass [Figs. 12(a and b)] were significantly deeper than those found within the valley regions (Fig. 11). This correlates with the lower strength of the EL series, which has a larger ridge

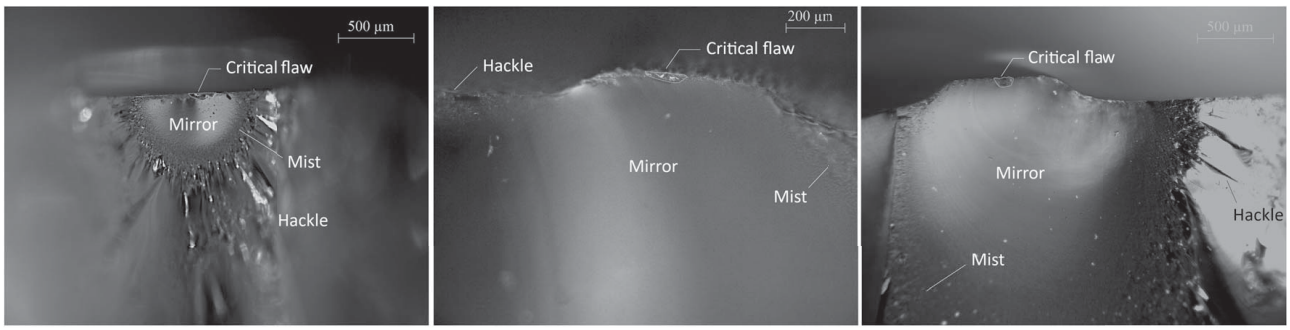

(a) (b) (c)

Fig. 10. Critical flaws in AR glass: (a) unetched float glass (U-AR); (b) etched diamond pattern glass (ED-AR); and (c) etched linear pattern glass (EL-AR).

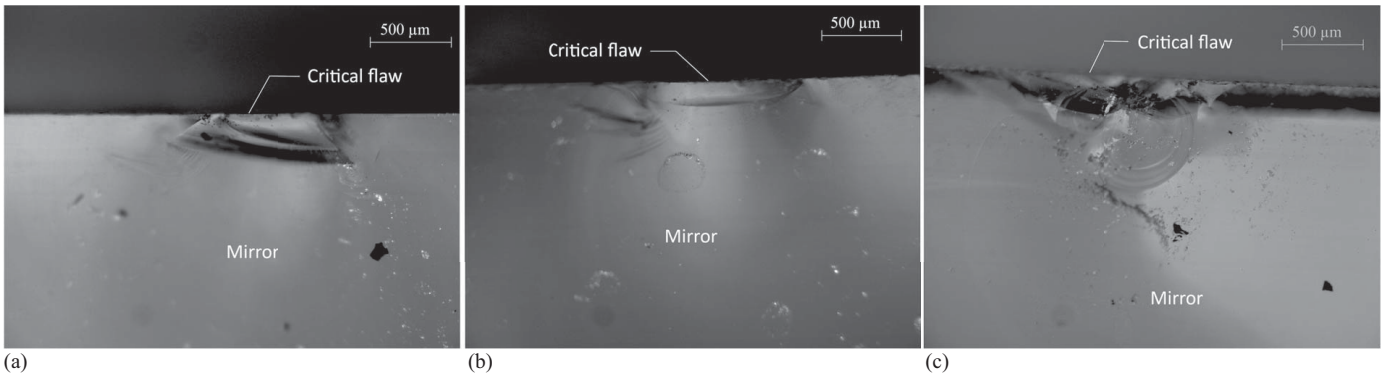

(a) (b) (c)

Fig. 11. Critical flaws in artificially aged glass: (a) unetched glass (U-AA); (b) etched diamond pattern glass (ED-AA); and (c) etched linear pattern glass (EL-AA).

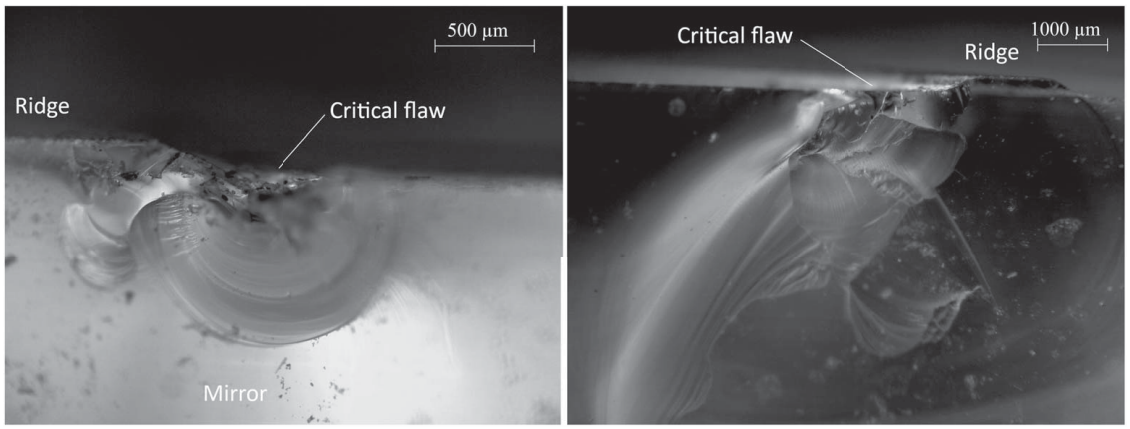

(a) (b)

Fig. 12. Critical flaws in artificially aged glass with gravel impact location at the root of the ridge: (a) etched diamond pattern glass (ED-AA); and (b) etched linear pattern glass (EL-AA).

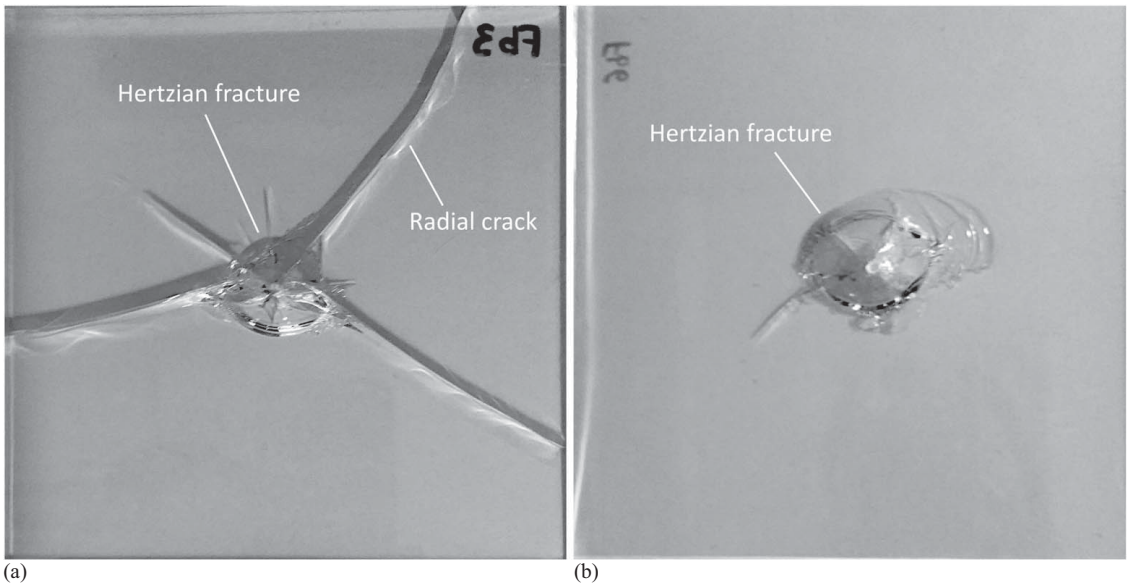

(a) (b)

Fig. 13. Hertzian fracture in unetched float glass: (a) complete fracture; and (b) localized fracture.

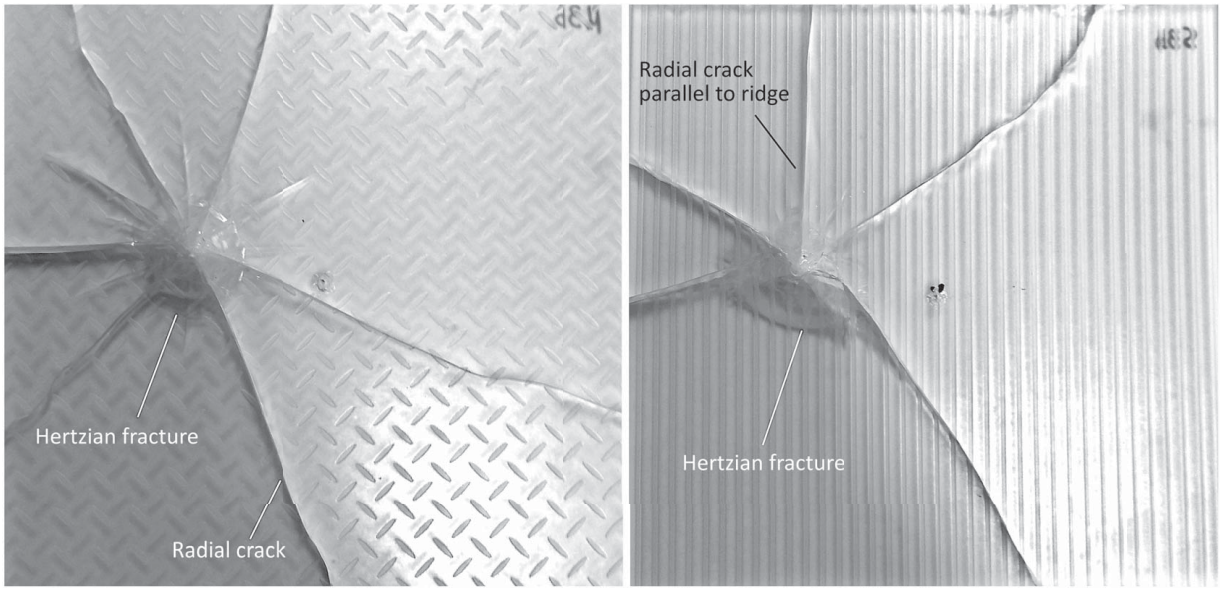

Fig. 14. Hertzian "valley" fracture for (a) ED glass; and (b) EL glass.

area than the ED series (section "Visual Inspection and Microscopy") and a correspondingly higher probability of gravel impact on the ridges.

Hertzian Fracture

Hertzian fractures in unetched float (U) glass generated radial cracks that propagated across the glass surface causing complete fracture of the specimen in five out of six glass specimens [Fig. 13(a)] while a localized Hertzian fracture was observed in the remaining specimen [Fig. 13(b)]. Radial cracks, originating from the Hertzian cone crack and resulting in complete fracture were generated for contact pressure on valley locations for the acid-etched specimens (Fig. 14). The cracks were randomly oriented for the diamond pattern glass (ED) [Fig. 14(a)]. Similar crack patterns were observed in all linear patterned glass (EL) except for two specimens where radial cracks formed parallel to the linear etch patterns [Fig. 14(b)].

Fracture patterns induced by Hertzian contact at the ridge locations of the acid-etched glass were distinctly different from those nucleating at valley locations; the ridge fractures were mainly localized Hertzian cones [Fig. 15(a)], with the exception of two out of six specimens of the acid-etched diamond pattern glass (ED) where the Hertzian cone was accompanied by a small number of radial cracks [Fig. 15(b)].

The loads applied to cause Hertzian fracture in the specimens are listed in Table 7. The corresponding stress, calculated from

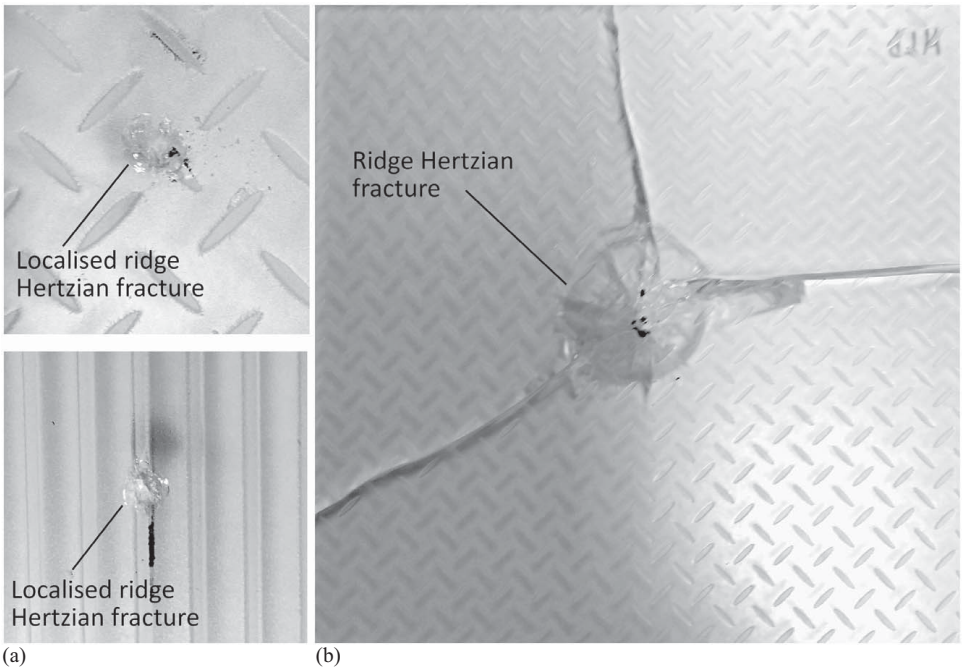

Fig. 15. Hertzian ridge fracture: (a) localized fractures for ED (top) and EL (bottom) glass; and (b) full fracture for ED glass.

Table 7. Fracture load and stress for Hertzian fracture tests

Series	a/a	Location	Load P (N)	Fracture stress $\sigma_{f,60}$ (MPa)
Unetched U glass	U-H1	NA	5,312.5	973.50
	U-H2	NA	5,518.8	985.94
	U-H3	NA	5,067.7	958.31
	U-H4	NA	5,164.6	964.38
	U-H5	NA	5,072.2	958.59
	U-H6	NA	5,099.9	960.34
	Mean	NA	5,206.0	966.8
Etched diamond ED glass	ED -Hv1	Valley	NA	NA
	ED-Hv2	Valley	6,364.6	1,033.93
	ED-Hv3	Valley	6,040.8	1,016.09
	ED-Hv4	Valley	NA	NA
	ED-Hv5	Valley	4,831.9	943.21
	ED-Hv6	Valley	4,970.2	952.12
	Mean	Valley	5,551.8	986.34
	ED-Hr1	Ridge	2,384.3	745.34
	ED-Hr2	Ridge	3,410.6	839.80
	ED-Hr3	Ridge	4,793.7	940.72
	ED-Hr4	Ridge	3,224.2	824.22
	ED-Hr5	Ridge	4,300.8	907.30
	ED-Hr6	Ridge	6,370.8	1,034.27
	Mean	Ridge	4,080.7	881.9
Etched linear EL glass	EL-Hv1	Valley	5,281.5	971.60
	EL-Hv2	Valley	5,351.9	975.90
	EL-Hv3	Valley	5,957.0	1,011.37
	EL-Hv4	Valley	6,223.2	1,026.22
	EL-Hv5	Valley	6,437.8	1,037.88
	EL-Hv6	Valley	4,543.4	924.05
	Mean	Valley	5,632.5	991.2
	EL-Hr1	Ridge	1,263.1	603.10
	EL-Hr2	Ridge	2,942.9	799.52
	EL-Hr3	Ridge	2,955.9	800.70
	EL-Hr4	Ridge	3,609.8	855.84
	EL-Hr5	Ridge	2,568.1	764.02
	EL-Hr6	Ridge	2,262.8	732.46
	Mean	Ridge	2,600.4	759.3

Eq. (9), was found to be very similar for the unetched float glass and both acid-etched glass types for "valley" contact pressures (967 MPa for F, 986 MPa for ED, and 991 MPa for EL glass) indicating negligible differences in fracture strength. However, the fracture strength for ridge contact on ED and EL glasses is 11% and 23% lower, respectively, compared to valley contact. These differences are likely to be due to a further geometric effect; in particular, the material in ridges is less confined compared with that found in the valleys, thereby being more susceptible to lateral fracture (bursting) under contact pressure. This indicates that ridges are weaker than valley regions, which agrees with the fractographic observations in the section "Fractography," which showed that the ridges had significantly deeper flaws than the valleys.

The lowest stress among all types of glass and tested locations was reported for the EL glass and contact pressure on the ridge. In particular, the EL glass was found to be 14% weaker than the ED glass for contact pressure at the ridge location. Similar to the abovementioned, this is potentially related to a geometric effect as ridges in EL glass are more pronounced/raised than ED glass [Figs. 6(b and d)]. Therefore, it is possible for local ridge bursting effects to occur at a lower load, as the material is less "confined" compared with the ED glass.

It should be noted that the fracture stress in Hertzian fracture tests is not directly proportional to the fracture load as the contact radius, ρ [Eq. (7)], is also a function of the fracture load. In addition and in contrast to the flexural strength data presented in the section "Destructive Tests and Strength Data," Hertzian fracture results refer to mean values as the small number of specimens did not permit a full statistical analysis.

There is a small scatter in fracture loads from the Hertzian tests at valley locations (coefficient of variation of 1.1%, 4.6%, and 4.3% for F, ED, and EL glass, respectively) while mean loads ranged between 5.2 and 5.6 kN for the three glass types. A much larger scatter was recorded for the ridge locations (coefficient of variation of 11.5% for both ED and EL glass) with mean loads of 2.6 and 4 kN for the EL and the ED series, respectively.

Previous research on staircase applied loads (Bougard 2002) showed that the dynamic load induced by pedestrians during normal operation, including fast descents, could be up to five times their own body weight (equating to an equivalent static load of 3.75 kN for a person of an average mass of 75 kg) while for abnormal use (e.g., for someone performing a standing jump), this factor can be up to 10 times their own self weight (i.e., 7.5 kN for a 75 kg person). This suggests that under normal use, it is possible for Hertzian fractures to appear in patterned annealed acid-etched glass when exposed to hard body contact pressure (e.g., grit/gravel pressed by pedestrian footwear onto a glass floor or staircase thread), particularly if the contact pressure is at the ridge of the acid-etched pattern. However, compression of the patterned acid-etched glass surface (e.g., from heat treatment) is expected to increase Hertzian fracture strength.

Conclusions

The aim of this study was to evaluate the fracture strength of acid-etched patterned glass, specifically when the glass is used as a horizontal surface that may be walked on by the general public (e.g., glass floors, glass staircase threads). In particular, the study investigated whether patterned glass has a lower surface tensile strength and/or a contact fracture strength than standard unetched float glass and whether the strength values of the etched patterned glass are especially sensitive to ageing.

A series of nondestructive, ageing, and destructive tests were therefore undertaken on three types of glass: two acid-etched glasses (one with a commonly used diamond pattern and one with a less-common linear pattern) and one type of unetched float annealed glass.

Micrographs of the AR glasses revealed that the acid treatment transforms the smooth surface of glass into a surface network of interconnected semispherical elevations, leading to light-scattering properties, and the associated frosted appearance, of the glass. The surface of the diamond pattern glass also contained several feather-shaped linear flaws that propagated from the ridge edges toward the valleys. No such flaws were found in the linear pattern glass. The root cause of these feather-shaped flaws is unknown, but strength data obtained from subsequent destructive tests indicate that these flaws have an insignificant effect on the strength of the glass and are inconsequential for engineering design purposes.

Controlled artificial ageing by gravel impact successfully induced flaws in all glass types, but the critical flaws found in the ridges and ridge/valley interfaces of the acid-etched glasses were significantly larger and deeper than those found on the valleys of the acid-etched glasses or the unetched float glass, indicating that the ridges constitute weak regions of the glass. This correlates with observations from microscopy findings prior to destructive testing, which revealed large digs (from gravel impacts) at these locations that are typically accompanied by radial median cracks.

Conversely, gravel impacts on valleys of the acid-etched glass revealed flaws of similar morphology and size to those observed in unetched float glass. However, it should be noted that fractographical analysis could only be performed on a small number of specimens.

The destructive flexural tests revealed that the mean surface tensile strength of AR acid-etched glass exceeds that of the AR unetched float glass, but there is a reversal in rank order at low probabilities of failure ($P_f = 0.008$) used in engineering design: where the AR unetched float glass was found to be 10% and 33% stronger than the diamond pattern glass and the linear pattern glass, respectively. This reversal is due to the larger scatter of strength data in the acid-etched glass relative to that of the unetched float glass. The surface tensile strength of the linear pattern glass falls below the 25% reduction threshold recommended in standards (BSI 2019). Flexural tests on the AA glass revealed that the mean surface tensile strengths of the three glasses are nearly identical, but that design surface tensile strength of the linear pattern glass is 15% lower than the other two glasses. The consistently lower surface tensile design strength of the linear pattern glass is attributed to the higher proportion of ridge areas relative to the total surface area, which increases the probability of a critical flaw (e.g., from gravel impact) located in these weaker areas.

From Hertzian fracture tests, it was found that there were no significant differences in the contact fracture strengths between the unetched float glass and the two acid-etched glasses, when the hard body contact was applied in the valley regions of the acid-etched glass. Conversely, significant reductions in contact fracture strengths were recorded for the acid-etched glass relative to the unetched glass strength (namely an 11% and a 23% reduction for the diamond pattern and the linear pattern, respectively) when the hard body contact was applied at the ridges. This corresponds to contact fracture load bearing capacities of 5,206, 4,080, and 2,600 N for the unetched, etched diamond pattern, and etched linear pattern, respectively. The expected range of dynamic point loads under normal pedestrian use in staircases (Bougard 2002) exceeded the contact fracture load bearing capacity of the etched linear pattern. Therefore, in practical applications, it is likely that Hertzian fractures will nucleate in acid-etched linear patterned glass unless hard body contact is prevented.

It is evident that ridge patterns weaken the glass compared with the flat material and could potentially lead to the formation of chips or localized Hertzian fractures. However, the antislip properties of patterned glass are beneficial for walking surfaces made of glass. Further studies should focus on: (1) distinguishing the optimal ratio of ridge area to the total surface area to provide a balance between friction and fracture resistance; and (2) identifying whether heat strengthening could improve the Hertzian fracture performance of patterned acid-etched glass.

Data Availability Statement

Some or all data, models, or code that support the findings of this study are available from the corresponding author upon reasonable request.

Acknowledgments

The authors wish to express their gratitude for the support received from the Structures Laboratory at the University of Cambridge during the execution of the tests performed in this study.

References

ASTM. 1991. *Standard test methods for abrasion resistance of organic coatings by falling abrasive*. ASTM D968-05. West Conshohocken, PA: ASTM.

ASTM. 2009. *Standard test method for monotonic equibiaxial flexural strength of advanced ceramics at ambient temperature*. ASTM C1499-03. West Conshohocken, PA: ASTM.

ASTM. 2016. *Standard practice for determining load resistance of glass in buildings*. ASTM E1300-16. West Conshohocken, PA: ASTM.

ASTM. 2021a. *Standard test method for relative resistance to wear of unglazed ceramic tile by the taber abraser*. ASTM C501-21. West Conshohocken, PA: ASTM.

ASTM. 2021b. *Standard specification for flat glass*. ASTM C1036-21. West Conshohocken, PA: ASTM.

Barboux, P., A. Laghzizil, Y. Bessoles, H. Deroulhac, and G. Trouvé. 2004. "Paradoxical crystalline morphology of frosted glass." *J. Non-Cryst. Solids* 345–346: 137–141. https://doi.org/10.1016/j.jnoncrysol.2004.08.011.

Bougard, A. 2002. "Human loading on staircases." *Proc. Inst. Civ. Eng. Struct. Build.* 152 (4): 371–380. https://doi.org/10.1680/stbu.2002.152.4.371.

BSI (British Standard Institution). 2019. *Glass in building - Determination of the lateral load resistance of glass panes by calculation*. BS EN 16612. London: BSI.

Dabbs, T. P., and B. R. Lawn. 1982. "Acid-enhanced crack initiation in glass." *J. Am. Ceram. Soc.* 65 (3): C-37–C-38. https://doi.org/10.1111/j.1151-2916.1982.tb10392.x.

Datsiou, K. 2017. "Design and performance of cold bent glass." Ph.D. thesis, Dept. of Engineering, Univ. of Cambridge.

Datsiou, K. C., and M. Overend. 2017. "Artificial ageing of glass with sand abrasion." *Constr. Build. Mater.* 142: 536–551. https://doi.org/10.1016/j.conbuildmat.2017.03.094.

Datsiou, K. C., and M. Overend. 2018. "Weibull parameter estimation and goodness-of-fit for glass strength data." *Struct. Saf.* 73: 29–41. https://doi.org/10.1016/j.strusafe.2018.02.002.

DIN (Deutsches Institut Fur Normung). 1985. *Standard for testing of glass and plastics; abrasion test; sand trickling method*. DIN 52348. Berlin: DIN.

Fischer-Cripps, A. C. 1997. "Predicting hertzian fracture." *J. Mater. Sci.* 32 (5): 1277–1285. https://doi.org/10.1023/A:1018500522014.

Frayret, J., O. Eterradossi, A. Castetbon, M. Potin-Gautier, G. Trouvé, and H. de Roulhac. 2008. "Determination of the correlation between physical measurements of roughness, optical properties, and perception of frosted glass surfaces." *Appl. Opt.* 47 (21): 3932–3940. https://doi.org/10.1364/AO.47.003932.

Haldimann, M., A. Luible, and M. Overend. 2008. *Structural use of glass*. Zurich, Switzerland: International Association for Bridge and Structural Engineering, IABSE Association.

Jang, H. K., Y. D. Chung, S. W. Whangbo, I. W. Lyo, C. N. Whang, S. J. Lee, and S. Lee. 2000. "Effects of chemical etching with hydrochloric acid on a glass surface." *J. Vac. Sci. Technol. A* 18 (5): 2563. https://doi.org/10.1116/1.1287445.

Kolli, M., M. Hamidouche, N. Bouaouadja, and G. Fantozzi. 2009. "HF etching effect on sandblasted soda-lime glass properties." *J. Eur. Ceram. Soc.* 29 (13): 2697–2704. https://doi.org/10.1016/j.jeurceramsoc.2009.03.020.

Lawn, B. 1993. *Fracture of brittle solids*. Cambridge: Cambridge University Press.

Maeng, J. H., D. H. Kim, S. M. Park, and H. J. Kim. 2014. "The effect of chemical treatment on the strength and transmittance of soda-lime cover glass for mobile." *Int. J. Precis. Eng. Manuf.* 15 (9): 1779–1783. https://doi.org/10.1007/s12541-014-0529-0.

Overend, M., and K. Zammit. 2012. "A computer algorithm for determining the tensile strength of float glass." *Eng. Struct.* 45: 68–77. https://doi.org/10.1016/j.engstruct.2012.05.039.

Piret, N., R. Santoro, L. Dogot, B. Barthélemy, E. Peyroux, and J. Proost. 2018. "Influence of glass composition on the kinetics of glass etching and frosting in concentrated HF solutions." *J. Non-Cryst.*

Solids 499 (June): 208–216. https://doi.org/10.1016/j.jnoncrysol.2018.07.030.
Quinn, G. 2007. *Fractography of ceramics and glasses*. Gaithersburg, MD: U.S. Government, National Institute of Standards and Technology.
Spierings, G. A. C. M. 1993. "Wet chemical etching of silicate glasses in hydrofluoric acid based solutions." *J. Mater. Sci.* 28 (23): 6261–6273. https://doi.org/10.1007/BF01352182.
Wang, Z., T. Guan, T. Ren, H. Wang, T. Suo, Y. Li, T. Iwamoto, X. Wang, Y. Wang, and G. Gao. 2020. "Effect of normal scratch load and HF etching on the mechanical behavior of annealed and chemically strengthened aluminosilicate glass." *Ceram. Int.* 46 (4): 4813–4823. https://doi.org/10.1016/j.ceramint.2019.10.214.
Wilshaw, T. 1971. "The Hertzian fracture test." *J. Phys. D: Appl. Phys.* 4: 1567. https://doi.org/10.1088/0022-3727/4/10/316.